DMD Fast Forward. Published on May 5, 2022 as DOI: 10.1124/dmd.122.000895
This article has not been copyedited and formatted. The final version may differ from this version.

Metabolic Activation of the Acrylamide Michael Acceptor Warhead in Futibatinib to an Epoxide Intermediate Engenders Covalent Inactivation of Cytochrome P450 3A

Lloyd Wei Tat Tang[1], Jiaxin Fu[1], Siew Kwan Koh[2], Guoyi Wu[1], Lei Zhou[2,3,4] and Eric Chun Yong Chan[1]

[1]Department of Pharmacy, Faculty of Science, National University of Singapore, Singapore

[2]Singapore Eye Research Institute (SERI), Singapore

[3]Department of Ophthalmology, Yong Loo Lin School of Medicine, National University of Singapore, Singapore

[4]Ophthalmology and Visual Sciences Academia Clinical Program, Duke-National University of Singapore Medical School, Singapore

DMD Fast Forward. Published on May 5, 2022 as DOI: 10.1124/dmd.122.000895
This article has not been copyedited and formatted. The final version may differ from this version.

Running Title:

Covalent Inactivation of CYP3A by Futibatinib

Address Correspondence to:

Professor Eric Chun Yong Chan, Department of Pharmacy, National University of Singapore, 18 Science Drive 4, Singapore 117543.

Email: phaccye@nus.edu.sg; Telephone: +65-6516 6137; Fax: +65-6779 1554

Number of Tables	4
Number of Figures	8
Number of References	33
Number of words in the Abstract	249
Number of words in the Significance Statement	79
Number of words in the Introduction	747
Number of words in the Discussion	1500

DMD Fast Forward. Published on May 5, 2022 as DOI: 10.1124/dmd.122.000895
This article has not been copyedited and formatted. The final version may differ from this version.

ABBREVIATIONS

CYP3A4	Cytochrome P450 3A4
CYP3A5	Cytochrome P450 3A5
DDI	Drug-drug interaction
FDA	United States Food and Drug Administration
FGFR	Fibroblast growth factor receptor
FUT	Futibatinib
GSH	Glutathione
G6P	Glucose-6-phosphate
G6PDH	Glucose-6-phosphate dehydrogenase
HPLC	High-performance liquid chromatography
K_I	Inactivator concentration at half-maximum inactivation rate constant
k_{inact}	Maximum inactivation rate constant
K_m	Michaelis constant
k_{obs}	Observed first-order rate constant of inactivation
IADR	Idiosyncratic adverse drug reactions
MBI	Mechanism-based inactivation
MIC	Metabolite-intermediate complex
MRM	Multiple reaction monitoring
P450	Cytochrome P450
rhCYP3A4	Recombinant human cytochrome P450 3A4
rhCYP3A5	Recombinant human cytochrome P450 3A5
ROS	Reactive oxygen species
$t_{1/2}$	Half-life
TDI	Time-dependent inhibition
UPLC-MS/MS	Ultra-high performance liquid chromatography tandem mass spectrometry

DMD Fast Forward. Published on May 5, 2022 as DOI: 10.1124/dmd.122.000895
This article has not been copyedited and formatted. The final version may differ from this version.

ABSTRACT

Futibatinib (FUT) is a potent inhibitor of fibroblast growth factor receptor (FGFR) 1-4 that is currently under clinical investigation for intrahepatic cholangiocarcinoma. Unlike its predecessors, FUT possesses an acrylamide warhead which enables it to bind covalently to a free cysteine residue in the FGFR kinase domain. However, it remains uninterrogated if this electrophilic *α,β*-unsaturated carbonyl scaffold could also directly or indirectly engender off-target covalent binding to nucleophilic centres on other cellular proteins. Here, we discovered that FUT inactivated both cytochrome P450 3A (CYP3A) isoforms with K_I, k_{inact}, and partition ratio of 12.5 and 51.4 μM, 0.25 and 0.06 min^{-1} and ~52 and ~58 for CYP3A4 and CYP3A5, respectively. Along with its time-, concentration- and cofactor-dependent inhibitory profile, FUT also exhibited several cardinal features that were consistent with mechanism-based inactivation. Moreover, the nature of inactivation was unlikely to be pseudo-irreversible and instead arose from the covalent modification of the P450 apoprotein and/or its heme moiety due to the lack of substantial enzyme activity recovery following dialysis and chemical oxidation as well as the absence of the diagnostic Soret peak in spectral analyses. Finally, utilizing GSH trapping and high-resolution mass spectrometry, we illuminated that while the acrylamide moiety in FUT could nonenzymatically conjugate to GSH via Michael addition, it was not implicated in the covalent inactivation of CYP3A. Rather, we surmised that it likely stemmed from the metabolic activation of its acrylamide covalent warhead to a highly electrophilic epoxide intermediate that could covalently modify CYP3A and culminate in its catalytic inactivation.

Keywords: bioactivation, covalent inhibition, CYP3A, epoxide, futibatinib, mechanism-based inactivation

DMD Fast Forward. Published on May 5, 2022 as DOI: 10.1124/dmd.122.000895
This article has not been copyedited and formatted. The final version may differ from this version.

SIGNIFICANCE STATEMENT

In this study, we reported for the first time the inactivation of CYP3A by FUT. Furthermore, using FUT as an exemplary targeted covalent inhibitor, our study revealed the propensity for its acrylamide Michael acceptor moiety to be metabolically activated to a highly electrophilic epoxide. Due to the growing resurgence of covalent inhibitors and the well-established toxicological ramifications associated with epoxides, we advocate that closer scrutiny be adopted when profiling the reactive metabolites of compounds possessing an *α,β*-unsaturated carbonyl scaffold.

DMD Fast Forward. Published on May 5, 2022 as DOI: 10.1124/dmd.122.000895
This article has not been copyedited and formatted. The final version may differ from this version.

INTRODUCTION

Pharmacological repression of fibroblast growth factor receptor (FGFR) signalling pathways is rapidly gaining scientific and therapeutic interest in cancer (Porta *et al.*, 2017). The impetus for this nascent treatment paradigm was ignited by a landmark genomic profiling study which revealed that FGFR genetic aberrations were prevalent in many solid tumours and subsequently corroborated by multiple lines of preclinical and clinical evidence which validated their oncogenic potential in independently driving tumorigenesis and conferring resistance mechanisms to existing anticancer therapies (Touat *et al.*, 2015; Helsten *et al.*, 2016). Currently, three FGFR-selective inhibitors have already garnered global regulatory approval; with many other promising candidates in advanced stages of clinical development (Chakrabarti *et al.*, 2022). Futibatinib (FUT) **(Fig. 1)**, previously designated as TAS-120, is one such drug that has been accorded Breakthrough Therapy designation by the U.S Food and Drug Administration (FDA) for the treatment of locally advanced or metastatic intrahepatic cholangiocarcinoma harbouring FGFR2-activating mutations (Goyal *et al.*, 2020).

Preliminary studies by the manufacturer have shown that FUT is chiefly metabolized by cytochrome P450 3A (CYP3A) – the most abundant cytochrome P450 enzyme (P450) isoform expressed in the liver (Yamamiya *et al.*, 2021). Collectively, the P450 represent a ubiquitous class of heme-containing enzymes that serve as one of the major drivers of xenobiotic oxidative metabolism in the human body (Guengerich, 2001). In fact, it is widely recognised that the metabolism of around eighty percent of all drugs marketed to-date can be ascribed to just six P450 isoforms (Zanger *et al.*, 2008). However, due to their wide substrate specificities and catalytic promiscuity, P450 may also inadvertently metabolically activate (or bioactivate) drug molecules to

DMD Fast Forward. Published on May 5, 2022 as DOI: 10.1124/dmd.122.000895
This article has not been copyedited and formatted. The final version may differ from this version.

electrophilic intermediates (Guengerich, 2011). These chemically-reactive species generated may then precipitate immune-mediated idiosyncratic adverse drug reactions (IADR) when liberated into the cellular milieu due to the wanton and indiscriminate alkylation to nucleophilic centres on biological macromolecules to form haptens which may constitute neoantigens that could elicit deleterious autoimmune responses (Masubuchi and Horie, 2007).

One other implication arising from metabolic activation that is germane to drug metabolism and disposition arises from the sequestration of the reactive intermediate within the enzymatic active site by means of covalent adduction to the P450 apoprotein and/or its heme moiety or through complexation with the catalytic ferrous (Fe^{2+}), thereby culminating in a distinctive time-dependent loss of its activity via a phenomenon known as mechanism-based inactivation (MBI) (Ho *et al.*, 2015). Unlike direct (or reversible) inhibition of P450, the loss of catalytic activity evoked by MBI is irreversible as the covalently-modified enzyme is irreparably inactivated and removed from the active pool of P450. Consequently, the MBI effects continue to persist even after the perpetrator has been systemically eliminated and abated only upon *de novo* protein synthesis. This explains why the likelihood and severity of drug-drug interactions (DDI) incited by an MBI tends to be more pronounced than with a direct inhibitor (Bjornsson *et al.*, 2003). Apart from its aforementioned time-dependent hallmark, an archetypal MBI is also known to exhibit these salient features: necessitation of a catalytically-competent system (i.e., presence of cofactors), saturable kinetics of inactivation, protection against inactivation by an alternative substrate or competitive inhibitor but not by exogenous nucleophilic scavengers, irreversibility of inactivation and a 1:1 binding stoichiometry (Silverman, 1995).

DMD Fast Forward. Published on May 5, 2022 as DOI: 10.1124/dmd.122.000895
This article has not been copyedited and formatted. The final version may differ from this version.

Our laboratory has recently established that the three FDA-approved FGFR inhibitors – namely erdafitinib, pemigatinib and infigratinib – elicited MBI of CYP3A (Tang *et al.*, 2021a; Tang *et al.*, 2021b; Tang *et al.*, 2022). Following which, we also deciphered the underlying metabolic activation pathways leading to the formation of the electrophilic intermediate(s) implicated in the covalent modification of the P450 apoprotein. Unlike its predecessors, FUT is a targeted covalent inhibitor that possesses an electrophilic acrylamide warhead which enables it to covalently bind to a unique free cysteine residue in the FGFR kinase domain (Sootome *et al.*, 2020). Although this has allowed it to elude drug resistance associated with conventional reversible ATP-competitive FGFR inhibitors, it may also increase its predisposition to cause off-target covalent binding. This factor, along with a previous report which revealed that FUT also inhibited CYP3A *in vitro* (Yamamiya *et al.*, 2021), led us to posit that FUT is metabolically activated to a reactive intermediate that engenders covalent inactivation of CYP3A.

In this study, we reported for the first time that FUT inactivates CYP3A4 and CYP3A5 in a time-, concentration- and cofactor-dependent manner consistent with MBI. Subsequently, glutathione (GSH) trapping experiments and high-resolution mass spectrometry revealed that FUT undergoes P450-mediated metabolic activation at its acrylamide Michael acceptor warhead to an epoxide intermediate which covalently inactivates CYP3A.

DMD Fast Forward. Published on May 5, 2022 as DOI: 10.1124/dmd.122.000895
This article has not been copyedited and formatted. The final version may differ from this version.

MATERIALS AND METHODS

Chemicals and Reagents. Erdafitinib and FUT were purchased from MedChem Express (Monmouth Junction, NJ). Catalase, dexamethasone, GSH, ketoconazole and rivaroxaban were procured from Sigma-Aldrich (St. Louis, MO). Potassium ferricyanide was acquired from VWR International (Leuven, Belgium). Human recombinant P450 3A4 and 3A5 Supersomes (rhCYP3A4 and rhCYP3A5) co-expressing both NADPH P450 oxidoreductase and cytochrome b_5 and the NADPH regenerating system comprising NADP+ and glucose-6-phosphate (G6P) (NADPH A) and glucose-6-phosphate dehydrogenase (G6PDH) (NADPH B) were commercially purchased from Corning Gentest (Woburn, MA). High performance liquid chromatography (HPLC)-grade acetonitrile was procured from Tedia Company Inc. (Fairfield, OH). Ultrapure water (type I) was prepared in our laboratory using a Milli-Q water purification system (Millipore Corporation, Bedford, MA).

Substrate Depletion of FUT by CYP3A. Triplicate incubation mixtures comprising 20 pmol/mL rhCYP3A4/5, FUT (1 μM), G6PDH and potassium phosphate buffer (100 mM; pH 7.4) were prepared and pre-warmed at 37°C for 5 min. Following which, the reaction was initiated via the addition of NADP+/G6P (final NADPH concentration 1 mM). At each predefined time interval (0, 5, 10, 15, 30, 45, 60, 80, 100 and 120 min), aliquots of each incubation mixture were withdrawn and added to an equal volume of ice-cold acetonitrile spiked with internal standard (0.1 μM erdafitinib) to stop the reaction. The quenched samples were then centrifuged at 4000*g* at 4°C for 30 min, after which the supernatant was withdrawn and analysed by ultra-high performance liquid chromatography-tandem mass spectrometry (UPLC-MS/MS) to quantify the amount of FUT remaining as previously described (Tang and Chan, 2022).

DMD Fast Forward. Published on May 5, 2022 as DOI: 10.1124/dmd.122.000895
This article has not been copyedited and formatted. The final version may differ from this version.

Time-, Concentration-, and NADPH-dependent Inactivation of CYP3A. CYP3A inactivation kinetic assays were performed as described in our recent works using the factor X_a direct anticoagulant rivaroxaban as a clinically-sensitive probe substrate of CYP3A (Tang *et al.*, 2021a; Tang *et al.*, 2021b; Tang *et al.*, 2022). Briefly, triplicate primary incubation mixtures comprising 40 pmol/mL rhCYP3A4/5, FUT (i.e., 0 – 25 μM for CYP3A4 incubations and 0 – 50 μM for CYP3A5 incubations), G6PDH and potassium phosphate buffer (100 mM; pH 7.4) were prepared and pre-warmed at 37°C for 5 min. Thereafter, the reaction was initiated via the addition of NADP+/G6P. Subsequently, at various preincubation intervals (i.e., 0, 3, 6, 9, 12 and 15 min), aliquots of each primary incubation mixture were withdrawn and diluted 20-fold into a pre-warmed secondary incubation mixture which consisted of saturating concentrations of rivaroxaban (50 μM; concentration corresponding to ~4× K_m), an NADPH regenerating system (1 mM) and potassium phosphate buffer (100 mM; pH 7.4). The secondary incubation mixtures were then further incubated for 2 h at 37°C. Following which, aliquots of the secondary incubation mixture were immediately withdrawn and added to an equal volume of ice-cold acetonitrile spiked with internal standard (4 μM dexamethasone). The quenched samples were then centrifuged at 4000*g* at 4°C for 30 min to obtain the supernatant for UPLC-MS/MS quantification of hydroxylated rivaroxaban which serves as a surrogate for the amount of CYP3A activity remaining **(Supplemental Methods; Supplemental Table 1)**. Negative control experiments were performed by replacing NADP+/G6P with potassium phosphate buffer (100 mM; pH 7.4).

Calculation of MBI Kinetic Parameters (K_I and k_{inact}). To derive the inactivator concentration at half-maximum inactivation rate constant (K_I) and maximum inactivation rate constant (k_{inact}), the means of triplicate peak area ratios were utilized

DMD Fast Forward. Published on May 5, 2022 as DOI: 10.1124/dmd.122.000895
This article has not been copyedited and formatted. The final version may differ from this version.

to calculate the natural logarithm of percentage P450 enzyme activity remaining normalized to vehicle which was then subsequently plotted against preincubation time for each FUT concentration. The resulting data points were fitted to linear regression and the observed first-order inactivation rate constant (k_{obs}) of FUT against CYP3A-mediated rivaroxaban hydroxylation was estimated from the slope of the initial linear decline in CYP3A activity for each FUT concentration. Specifically, points from preincubation timepoints 0 to 12 min were adopted in the calculation of the k_{obs} in CYP3A4 incubations due to a loss of linearity occurring at 15 min timepoint. Conversely in CYP3A5 incubations, points throughout 0 to 15 min were utilized as the decline in enzymatic activity was determined to be linear throughout. After which, a plot of k_{obs} against FUT concentrations [*I*] allowed the fitting of inactivation kinetic constants (K_I and k_{inact}) to nonlinear least square regression based on **Equation 1** in GraphPad 8.0.2 (San Diego, CA)

$$k_{\mathrm{obs}} = \frac{k_{\mathrm{inact}} \times [I]}{K_{\mathrm{I}} + [I]} \quad (1)$$

Equation 1 assumes that the change of [*I*] during the preincubation period is negligible and that the loss of enzymatic activity purely stems from inactivation by FUT. Moreover, it was also assumed that the nonspecific binding of FUT to rhCYP3A4/5 in the preincubation incubation mixtures was minimal hence the apparent K_I values described in this work were derived from total drug concentrations rather unbound drug concentrations. The k_{inact}/K_I ratio was determined by dividing the mean values of k_{inact} by K_I. Lastly, the time required for half of the enzyme molecules to be inactivated ($t_{1/2}$) was determined by **Equation 2**.

DMD Fast Forward. Published on May 5, 2022 as DOI: 10.1124/dmd.122.000895
This article has not been copyedited and formatted. The final version may differ from this version.

$$t_{1/2} = \frac{ln2}{k_{\text{inact}}} \quad (2)$$

Partition Ratio. Triplicate primary incubation mixtures consisting of 100 pmol/mL rhCYP3A4/5, FUT (0, 1, 2.5, 5, 15, 25 and 50 μM), G6PDH and potassium phosphate buffer (100 mM; pH 7.4) were prepared, pre-warmed at 37°C for 5 min and the reaction was subsequently initiated via the addition of NADP+/G6P. The reaction mixtures were incubated for a protracted duration of 45 min to allow CYP3A inactivation by FUT to go into completion. Thereafter, aliquots of the primary incubation mixture were withdrawn and diluted 20-fold into the pre-warmed secondary incubation mixture (similar to that prepared for the aforementioned inactivation assays) and incubated at 37°C for a further 2 h. Samples were then quenched, centrifuged and assayed for residual CYP3A enzyme activity by UPLC-MS/MS **(Supplemental Methods)**. The turnover number and partition ratio was computed as outlined in our previous study (Tang *et al.*, 2021c). Briefly, the percentage of residual CYP3A activity was plotted against the molar ratio of FUT to CYP3A concentration (i.e., 0 – 500). The turnover number was computed by determining the intercept of the straight line plotted at lower molar ratios with the linear regression line plotted at higher molar ratios to the abscissa. Finally, the partition ratio was back calculated by subtracting the turnover number by a numerical value of 1.

Substrate Protection. To investigate if enzyme inactivation was amenable to substrate protection, an alternative CYP3A substrate (testosterone) or a potent direct inhibitor of CYP3A (ketoconazole) was individually introduced into the reaction mixtures. Briefly, triplicate primary incubation comprising 40 pmol/mL rhCYP3A4/5, FUT (25 μM), G6PDH, potassium phosphate buffer (100 mM; pH 7.4) and either

DMD Fast Forward. Published on May 5, 2022 as DOI: 10.1124/dmd.122.000895
This article has not been copyedited and formatted. The final version may differ from this version.

testosterone (100 and 200 μM; equivalent to 1:4 and 1:8 molar ratio of FUT:testosterone) or ketoconazole (0.1 and 1 μM; corresponding to ~1× and ~10× its K_i value) were prepared. The reaction was initiated via the addition of NADP+/G6P after pre-warming at 37°C for 5 min. Aliquots were withdrawn at different preincubation time points (i.e. 0, 3, 6 and 9 min for CYP3A4 incubations and 0, 6, 12 and 15 min for CYP3A5 incubations), transferred to the secondary incubation mixture and subsequently quenched, centrifuged and assayed for residual CYP3A enzymatic activity by UPLC-MS/MS **(Supplemental Methods)**. Primary incubation mixtures that omitted the addition of either testosterone, ketoconazole or both FUT and testosterone or ketoconazole served as the negative controls.

Effect of Exogenous Nucleophile and Scavenger of ROS on Inactivation. Triplicate primary incubation mixture containing 40 pmol/mL rhCYP3A4/5, FUT (25 μM), G6PDH and potassium phosphate buffer (100 mM; pH 7.4) were individually enriched with either GSH (2 mM) or catalase (800 U/mL) – which were employed as an exogenous nucleophile and scavenger of ROS respectively. After pre-warming at 37°C for 5 min, the enzymatic reaction was initiated via the addition of NADP+/G6P. At specific preincubation time points (i.e. 0, 3, 6 and 9 min for CYP3A4 incubations and 0, 6, 12 and 15 min for CYP3A5 incubations), aliquots were transferred to the secondary incubation mixtures and subsequently quenched, centrifuged and assayed for residual CYP3A enzymatic activity by UPLC-MS/MS **(Supplemental Methods)**. Primary incubation mixtures that obviated the addition of either GSH or catalase or both FUT and GSH or catalase served as the negative controls.

Reversibility of Inactivation. The reversibility of CYP3A inactivation was evaluated by two complementary methodologies; namely dialysis and chemical oxidation by

DMD Fast Forward. Published on May 5, 2022 as DOI: 10.1124/dmd.122.000895
This article has not been copyedited and formatted. The final version may differ from this version.

potassium ferricyanide, as expounded in greater detail in our previous works (Tang *et al.*, 2021b; Tang *et al.*, 2022). In the first series of experiments involving dialysis, triplicate primary incubation mixtures comprising 40 pmol/mL rhCYP3A4/5, FUT (0 or 25 μM), G6PDH and potassium phosphate buffer (100 mM; pH 7.4) were preincubated at 37°C for 5 min. Enzymatic reaction was initiated by the addition of NADP+/G6P and allowed to proceed for 30 min. After which, a 5 μL aliquot was transferred to the secondary incubation mixture yielding a 20-fold dilution. Concurrently, the remaining primary incubation mixture (approximately 90 μL) was transferred to a Slide-A-Lyzer mini dialysis device (molecular weight cutoff of 10,000; Pierce Chemical Co., Rockford, IL) and gently lowered into a glass beaker filled with 500 mL of ice-cold potassium phosphate buffer (100 mM; pH 7.4). The buffer system was maintained on ice (4°C) with constant gentle stirring and accompanied by one fresh buffer change at the second hour mark. After 4 h, a 5 μL aliquot of the dialyzed mixture was transferred to each pre-warmed secondary incubation well. All secondary mixtures were further incubated at 37°C for 2 h and subsequently assayed for residual CYP3A enzymatic activity by UPLC-MS/MS **(Supplemental Methods)**.

In the second series of experiments involving chemical oxidation with potassium ferricyanide, three sequential incubations were performed. Briefly, the primary incubation consisted of 40 pmol/mL rhCYP3A4/5, FUT (0 or 25 μM), G6PDH and potassium phosphate buffer (100 mM; pH 7.4). Following the initiation of the reaction with the addition of NADP+/G6P and incubation at 37°C for either 0 or 30 min, 20 μL of the primary incubation mixture was aliquoted into an equal volume of secondary incubation mixture containing potassium phosphate buffer (100 mM; pH 7.4) with or without potassium ferricyanide (2 mM). The secondary mixtures were then allowed to

DMD Fast Forward. Published on May 5, 2022 as DOI: 10.1124/dmd.122.000895
This article has not been copyedited and formatted. The final version may differ from this version.

incubate at 37°C for another 10 min. Thereafter, 10 µL of the mixture was withdrawn and diluted 10-fold into a tertiary incubation mixture containing rivaroxaban (50 µM), an NADPH regenerating system (1 mM) and potassium phosphate buffer (100 mM; pH 7.4). The reaction mixture was further incubated at 37°C for another 2 h and subsequently assayed for residual CYP3A activity by UPLC-MS/MS **(Supplemental Methods)**. The percentage of CYP3A metabolic activity remaining after 0 or 30 min incubation with FUT compared to the corresponding controls in the absence of FUT was calculated using **Equation 3** and **4** respectively.

$$\%\ \text{control}_{0\ min} = \frac{v_{\ (0\ \text{min},(+)\ FUT)}}{v_{\ (0\ \text{min},\ (-)\ FUT)}} \times 100 \quad (3)$$

$$\%\ \text{control}_{30\ min} = \frac{v_{\ (30\ \text{min},(+)\ FUT)}}{v_{\ (30\ \text{min},(-)\ FUT)}} \times 100 \quad (4)$$

where v represents the residual CYP3A activity. Thereafter, % restoration of metabolic activity of CYP3A was derived by subtracting % $\text{control}_{30\ min}$ in the presence of potassium ferricyanide with the corresponding values obtained in the absence of potassium ferricyanide.

Spectral Difference Scanning. Incubation mixtures containing 200 pmol/mL rhCYP3A4/5, FUT (25 µM), G6PDH and potassium phosphate buffer (100 mM; pH 7.4) were prepared, pre-warmed at 37°C for 5 min and initiated via the addition of NADP+/G6P. At the same time, it was immediately scanned from 400 to 500 nm at 5 min intervals over a 1 h duration using a Hidex Sense microplate reader (Hidex, Turku, Finland) thermostated at 37°C. The spectral differences were obtained by comparing the UV absorbances between the sample and reference wells which consisted of vehicle in place of FUT. Additionally, the degree of metabolite-

DMD Fast Forward. Published on May 5, 2022 as DOI: 10.1124/dmd.122.000895
This article has not been copyedited and formatted. The final version may differ from this version.

intermediate complex (MIC) formation was also semi-quantitatively assessed by measuring the absorbance difference between 454 and 490 nm with time.

GSH Trapping Assay. GSH trapping experiments were performed as previously described with minor modifications (Tang *et al.*, 2021a; Tang *et al.*, 2021b). Incubation mixtures containing 50 pmol/mL rhCYP3A4, FUT (25 μM), G6PDH and potassium phosphate buffer (100 mM; pH 7.4) were fortified with GSH (50 mM) and pre-warmed at 37°C for 5 min. The reaction was then initiated via the addition of NADP+/G6P and incubated at 37°C for 1 h. After which, an equal volume of ice-cold acetonitrile was added to quench the reaction. The resulting mixture was centrifuged at 14,000*g* at 4°C for 15 min. Following which, the supernatant was transferred to a new microcentrifuge tube and concentrated using a gentle stream of nitrogen gas (TurboVap LV; Caliper Life Science, Hopkinton, MA). The residue was subsequently reconstituted with 60 μL of ACN-water mixture (3:7), vortexed and centrifuged at 14,000*g* at 4°C for 15 min. The resulting supernatant was then carefully removed and transferred to a fresh vial to detect FUT-derived GSH adducts via UPLC-MS/MS. Samples which omitted the inclusion of FUT or rhCYP3A4 in the incubation mixture served as the vehicle and enzyme-free controls, respectively.

Detection of GSH Adducts by UPLC-MS/MS. GSH adducts of FUT formed *in situ* in the GSH trapping assay were detected using the UPLC-MS/MS system comprising an Agilent 1290 Infinity ultra-high pressure liquid chromatography (Agilent Technologies Inc., Santa Clara, CA) interfaced with a triple quadrupole linear ion trap mass spectrometer (AB SCIEX QTRAP 5500 MS system equipped with a Turbo V ion source; AB SCIEX, Framingham, MA). Chromatographic separation was achieved on an ACQUITY UPLC ethylene bridged hybrid C_{18}, 2.2 ×

DMD Fast Forward. Published on May 5, 2022 as DOI: 10.1124/dmd.122.000895
This article has not been copyedited and formatted. The final version may differ from this version.

100 mm, 1.7 µM column (Waters, Milford, MA) using 0.1% formic acid in water (A) and 0.1% formic acid in acetonitrile as the mobile phases. Mobile phases were delivered at a flow rate of 0.35 mL/min. The column and sample temperature were set at 45°C and 4°C respectively. The gradient elution conditions were as follows: isocratic at 10% B (0 – 2.00 min), linear gradient 10 to 70% B (2.01 – 12.00 min), linear gradient 70 to 90% B (12.01 – 14.00 min), isocratic at 90% B (14.01 – 18.00 min), isocratic at 10% B (18.01 – 20.00 min). An information-dependent acquisition experiment was conducted to detect FUT-derived GSH conjugates using two well-established survey scans; namely precursor ion scan (PIS) of *m/z* 272 in negative ESI mode and constant neutral loss scan (NL) of 129 Da in positive ESI mode. Enhanced product ion (EPI) scan was subsequently performed for all putative GSH adducts identified in positive ESI mode. The source-dependent MS parameters utilized were as follows: ion spray voltage = 4500 V; source temperature = 500°C; curtain gas (CUR) = 30 psi; ion source gas 1 (sheath gas) = 50 psi; ion source gas 2 (drying gas) = 50 psi.

Following which, the accurate masses of the GSH adducts prospectively identified by the aforementioned QTRAP-MS was measured using an ACQUITY ultra-high pressure liquid chromatography (Waters, Milford, MA) coupled to an Orbitrap Exploris 480 MS (Thermo Fisher Scientific, San Jose, CA). The C_{18} column, mobile phases, flow rate, temperature and gradient elution conditions were identical to those described earlier in this section. The injection volume was 3 µL and the analytes were ionized by ESI in positive ion mode under the following conditions: sheath gas: 50 arbitrary units; auxiliary gas: 10 arbitrary units; sweep gas: 1 arbitrary unit; S-lens: 50; ion transfer tube temperature: 325°C; vaporizer temperature: 350°C, whereas a normalized collision energy of 20% was applied to fragment all ions. The Orbitrap-

DMD Fast Forward. Published on May 5, 2022 as DOI: 10.1124/dmd.122.000895
This article has not been copyedited and formatted. The final version may differ from this version.

MS data were acquired and further processed using Xcalibur 4.4 and Freestyle 1.7 software (Thermo Fisher Scientific, San Jose, CA).

DMD Fast Forward. Published on May 5, 2022 as DOI: 10.1124/dmd.122.000895
This article has not been copyedited and formatted. The final version may differ from this version.

RESULTS

Substrate Depletion of FUT in CYP3A. While FUT was previously reported to inhibit CYP3A *in vitro* (Yamamiya *et al.*, 2021), the exact biochemical nature underscoring its inhibition remains obfuscated. Consequently, in order to evaluate if FUT elicits any considerable TDI of CYP3A, we first monitored the depletion of 1 μM FUT in rhCYP3A4/5 over a period of 2 h. Our findings corroborated earlier reports by the manufacturer that FUT is predominantly metabolized by CYP3A due to the rapid turnover of FUT observed in our substrate depletion assay (Yamamiya *et al.*, 2021). Notably, FUT appeared to be metabolized more efficiently by CYP3A4 – with 11.8 ± 1.4% of the parent drug remaining after a 1 h incubation with rhCYP3A4 **(Fig. 2A)** as compared to 39.8 ± 2.5% in rhCYP3A5 incubations **(Fig. 2B)**. Applying a log transformation gave rise to two distinct linear phases in the substrate depletion profile of FUT in CYP3A4 **(Fig. 2C)**, whereas a single linear phase was observed for that of CYP3A5 **(Fig. 2D)**. Consequently, two different elimination rate constants (termed $k_{fast,3A4}$ and $k_{slow,3A4}$) were calculated for CYP3A4. Juxtaposing the elimination rate constant for CYP3A4 obtained in the initial portion of incubation with that of CYP3A5 revealed that FUT was metabolized ~3 times faster by CYP3A4 as compared to CYP3A5 (i.e., $k_{fast,3A4}$ = 0.041 ± 0.001 min^{-1} compared with k_{3A5} = 0.014 ± 0.001 min^{-1}). However, after about 1 h, there was a marked reduction in the elimination rate constant of FUT by CYP3A4 (i.e., $k_{slow,3A4}$ = 0.017 ± 0.001 min^{-1}) which seems to suggest that either significant loss of the substrate has occurred or that TDI (or inactivation) of the enzyme had taken place.

Time-, Concentration-, and Cofactor-dependent Inactivation of CYP3A by FUT. We then proceeded to quantitatively investigate its inactivation kinetics using

DMD Fast Forward. Published on May 5, 2022 as DOI: 10.1124/dmd.122.000895
This article has not been copyedited and formatted. The final version may differ from this version.

rivaroxaban – a clinically-sensitive probe of CYP3A. Our findings confirmed that FUT inactivated CYP3A4-mediated rivaroxaban hydroxylation in a time- and concentration-dependent manner **(Fig. 3A)** – with the greatest loss of rivaroxaban hydroxylase activity attained when 25 μM FUT was preincubated for 15 min with CYP3A4. Moreover, as the k_{obs} of FUT against CYP3A4 tended towards a maximum rate (i.e., k_{inact}) **(Fig. 3B)**, it denoted that the loss of CYP3A4 activity elicited by FUT is saturable and exhibited pseudo-first-order kinetics. The K_I and k_{inact} of FUT derived from the Kitz-Wilson plot (Kitz and Wilson, 1962) were determined to be 12.5 ± 2.4 μM and 0.25 ± 0.02 min^{-1} respectively which in turn yielded a k_{inact}/K_I ratio of 20.0 $min^{-1}mM^{-1}$ and inactivation $t_{1/2}$ of 2.8 min. Furthermore, the exclusion of NADPH – which serves as an important cofactor in P450-mediated metabolic reactions – completely nullified the loss of CYP3A4-mediated rivaroxaban hydroxylase activity by FUT **(Fig. 3C)**, thereby indicating that metabolic activation of FUT was an instrumental preceding molecular event that is necessary for enzyme inactivation. Unexpectedly, parallel experiments with CYP3A5 also revealed that FUT elicited time-, concentration- and cofactor-dependent inactivation of CYP3A5-mediated rivaroxaban hydroxylation with K_I and k_{inact} values of 51.4 ± 21.4 μM and 0.06 ± 0.02 min^{-1} respectively **(Supplemental Fig. 1A – C)**. This in turn translated to a k_{inact}/K_I ratio of 1.2 $min^{-1}mM^{-1}$ and an inactivation $t_{1/2}$ of 11.6 min. Taken together, our results revealed that the inactivation of CYP3A5 by FUT was approximately ~16.7 times less potent than that of CYP3A4 which could have explained why the earlier substrate depletion plot for CYP3A5 did not exhibit a biphasic profile akin to that of CYP3A4. All values of K_I, k_{inact}, k_{inact}/K_I ratio and $t_{1/2}$ reported in this work are summarized in **Table 1**.

DMD Fast Forward. Published on May 5, 2022 as DOI: 10.1124/dmd.122.000895
This article has not been copyedited and formatted. The final version may differ from this version.

Partition Ratio. The partition ratio is an estimate of the number of inactivator molecules that are metabolized and liberated from the enzymatic site without causing inactivation relative to each molecule of the enzyme that gets inactivated (Orr *et al.*, 2012). Adopting a previously described titration method (Silverman, 1995), the turnover number for the inactivation of CYP3A4 and CYP3A5 by FUT was found to be approximately ~53 and ~59 respectively **(Fig. 4A) (Supplemental Fig. 2A)**. This in turn corresponded to a partition ratio of ~52 for CYP3A4 and ~58 for CYP3A5 **(Table 1)**.

Substrate Protection. The inactivation of CYP3A4 by FUT was attenuated in a dose-dependent manner by the coincubation of testosterone, an alternative substrate of CYP3A **(Fig. 4B)**. Similarly, the incorporation of the potent CYP3A direct inhibitor ketoconazole at a concentration of 0.1 μM also diminished the rate of inactivation **(Fig. 4C)**. However, unlike with testosterone, enzyme inactivation was abolished when 1 μM ketoconazole was coincubated with FUT and CYP3A4 in the primary incubation mixture, thereby denoting that complete protection against inactivation had taken place. Similarly, these trends in substrate protection were also recapitulated in CYP3A5 **(Supplemental Fig. 2B and C)**.

Effect of Exogenous Nucleophile and Scavenger of ROS on Inactivation. On the contrary, the inclusion of GSH and catalase did not offer any appreciable protection from inactivation, wherein CYP3A4 and CYP3A5 was inactivated to a similar extent as incubation mixtures comprising FUT alone **(Fig. 4D) (Supplemental Fig. 2D)**.

Reversibility of Inactivation. Dialysis and chemical oxidation with potassium ferricyanide was conducted to delineate the specific nature of inactivation of CYP3A

DMD Fast Forward. Published on May 5, 2022 as DOI: 10.1124/dmd.122.000895
This article has not been copyedited and formatted. The final version may differ from this version.

by FUT (i.e., pseudo-irreversible or irreversible). The results of the first series of experiments revealed an absence of CYP3A activity recovery following dialysis at 4°C for 4 h **(Fig 5A) (Supplemental Fig. 3A)**. At this juncture, it should be noted that the marginal drop in the remaining enzyme activity observed after dialysis could be explained by enzymatic degradation that occurred during the course of dialysis. In the second series of experiments, potassium ferricyanide only modestly restored the metabolic activity of CYP3A4 and CYP3A5 by 1.3 ± 0.3% and 5.6 ± 1.3% respectively after a 30 min preincubation with 25 μM FUT **(Fig. 5B) (Supplemental Fig. 3B)** – which was grossly under the predefined threshold of 20% for MIC-forming inactivators (Watanabe *et al.*, 2007).

Spectral Difference Scanning. To further substantiate the proposed mechanism of inactivation evoked by FUT against CYP3A, spectral difference scanning was performed. The results of these experiments revealed that the absorbance difference measured in CYP3A4 incubations over a 1 h duration failed to detect a spectrally resolvable peak in the Soret region (448 – 458 nm) commonly associated with MIC **(Fig. 5C)** (Polasek and Miners, 2008). Moreover, tracking the increase in absorbance between 454 nm and the isosbestic point at 490 nm against time further corroborated the lack of MIC formation with FUT **(Fig. 5D)**. Likewise, these observations were also consistent in parallel experiments conducted with CYP3A5 **(Supplemental Fig. 3C and D)**.

GSH Trapping. A GSH trapping assay was conducted to profile reactive intermediates which could have perpetrated covalent modification of CYP3A leading to its inactivation. Here, we adopted the well-established PIS at *m/z* 272 in negative mode and constant NL scan of 129 Da in positive mode – which monitors for the loss

DMD Fast Forward. Published on May 5, 2022 as DOI: 10.1124/dmd.122.000895
This article has not been copyedited and formatted. The final version may differ from this version.

of the deprotonated γ-glutamyl-dehydroalanyl-glycine and pyroglutamic acid moiety from GSH respectively (Baillie and Davis, 1993; Dieckhaus *et al.*, 2005). Notably, these survey scans evinced two peaks suggestive of FUT-derived GSH adducts; namely FUT-G1 (retention time: 6.32 min) and FUT-G2 (retention time: 6.24 min) with $[M+H]^+$ ion at *m/z* of 726.1 and 742.3 respectively, that were absent in vehicle-containing samples (**Fig. 6A and D)** and only detected in incubation mixtures comprising FUT **(Fig. 6B and E)**. Intriguingly, we were unable to detect the less abundant FUT-G2 peak when rhCYP3A4 was replaced with potassium phosphate buffer **(Fig. 6C and F)**. The resultant EPI MS/MS spectra further reinforced our postulations that both these peaks corresponded to GSH adducts due to its characteristic collision-induced dissociation fragmentation pattern yielding neutral mass loss of 129 Da (corresponding to the loss of a pyroglutamate moiety) **(Supplemental Fig. 4A – D)**. After which, accurate mass measurements were performed to definitely elucidate the structures of FUT-G1 and FUT-G2. As expected, we were able to recapitulate the nominal mass patterns generated using the QTRAP-MS when the GSH conjugates were subjected to accurate mass measurements using the Orbitrap-MS. The proposed elemental composition, theoretical and experimental exact *m/z* and mass accuracy (in both ∆Da and ∆ppm) of FUT-G1 and FUT-G2 are outlined in **Table 2 and 3** respectively. Additionally, the representative product ion chromatogram, accurate mass MS/MS spectrum and proposed fragmentation pattern of FUT-G1 and FUT-G2 are illustrated in **Fig. 7A – D**.

DMD Fast Forward. Published on May 5, 2022 as DOI: 10.1124/dmd.122.000895
This article has not been copyedited and formatted. The final version may differ from this version.

DISCUSSION

FUT is a novel irreversible inhibitor of FGFR1-4 that is currently under clinical investigation for intrahepatic cholangiocarcinoma. Although early studies have reported that FUT inhibits CYP3A *in vitro*, the exact biochemical nature underpinning its inhibition profile remains nebulous. Here, our study revealed that FUT inactivated CYP3A-mediated rivaroxaban hydroxylation in a manner that is consistent with MBI. Thereafter, using high-resolution mass spectrometry, we illuminated that FUT is amendable to metabolic activation at its acrylamide moiety to an unstable epoxide intermediate that is likely implicated in the covalent inactivation of CYP3A.

From a drug discovery standpoint, inactivators which possesses a larger k_{inact} and a smaller K_I value generally have a larger propensity to elicit DDI *in vivo*. Consequently, the k_{inact}/K_I ratio is frequently employed as a metric to quantitatively assess the *in vitro* inactivation potency of a preclinical drug candidate (Orr *et al.*, 2012). Comparing the k_{inact}/K_I ratios derived for CYP3A4 revealed that the inactivation potency of FUT was in the same order of magnitude as the other FDA-approved FGFR inhibitors **(Table 4)**. Moreover, the apparent k_{obs} for CYP3A4 and CYP3A5 at 10 μM was calculated to be 0.11 min^{-1} and 0.01 min^{-1} respectively, thereby implying that only the inactivation of CYP3A4 is likely to constitute a potential *in vivo* pharmacokinetic DDI risk (Zimmerlin *et al.*, 2011). Unfortunately, a more precise estimation of its DDI risk cannot be evaluated at this point of time as FUT is still an investigational drug. Consequently, there is a dearth of other relevant drug-dependent parameters in the scientific literature or public domain. Another important parameter of an MBI is its partition ratio which is widely regarded as a quantitative measure of its inactivation efficiency. While the exact mechanistic basis underscoring the differential efficiencies is contingent on a complex interplay of

DMD Fast Forward. Published on May 5, 2022 as DOI: 10.1124/dmd.122.000895
This article has not been copyedited and formatted. The final version may differ from this version.

biochemical factors such as the intrinsic reactivity of the intermediate formed and the adjacency to its intended substructural target within the enzymatic active site (Nassar *et al.*, 2008), there is broad consensus that inactivators possessing partition ratios under 50 are highly efficient (Lim *et al.*, 2005). Consequently, our findings implied that the inactivation of CYP3A4 by FUT is only moderately efficient and pales in comparison to those obtained for the other three FDA-approved FGFR inhibitors **(Table 4)**. Furthermore, while the coincubation with scavenger nucleophiles (i.e., GSH and catalase) afforded virtually no protection against inactivation it is starkly contrasted with the incorporation of testosterone or ketoconazole – which markedly attenuated the observed rate of inactivation. These findings shed some light into its molecular determinants by further substantiating that inactivation likely occurred within its active site and thus could be protected by a competing substrate or a potent inhibitor. Importantly, these results also ruled out potentially confounding artefactual causes of inactivation (i.e., production of ROS in the P450 catalytic cycle) and are well-aligned with our earlier postulation that the time-dependent loss of enzymatic activity engendered by FUT stemmed from a putative reactive intermediate that is formed via P450-mediated metabolic activation.

Following which, a series of three experiments were performed to decipher if CYP3A inactivation arose through a MIC or via covalent modification. In broad strokes, MIC results from the chelation of the heme catalytic ferrous by the chemically-reactive intermediate via a strong coordinate bond. While such coordination complexes are stable *in vivo*, they may be dissipated under certain *in vitro* conditions which allows them to distinguished experimentally. This is commonly achieved via dialysis or chemical oxidation using potassium ferricyanide which reverts the heme iron back to its reduced ferric ground state and in doing so liberates it from the tight-binding

DMD Fast Forward. Published on May 5, 2022 as DOI: 10.1124/dmd.122.000895
This article has not been copyedited and formatted. The final version may differ from this version.

complex with the inactivator and restores its catalytic activity. This explains why MIC are termed as pseudo-irreversible. Conversely, covalent alkylation of the P450 apoprotein and/or prosthetic heme culminates in an irrevocable loss of enzyme activity that cannot be alleviated by both aforementioned methodologies. Notably, aniline-based drugs like dapsone and procainamide have previously been reported to be capable of undergoing P450-mediated oxidation to a labile nitroso intermediate which is capable of forming of a MIC (Kalgutkar *et al.*, 2007). As FUT similarly possesses an anilyl moiety, it was imperative to interrogate if it elicited any pseudo-irreversible inactivation of CYP3A. Here, results from all three assays were in concordance and collectively asserted that the nature of inactivation of CYP3A by FUT was unlikely to be pseudo-irreversible and instead arose from the covalent modification of the P450 apoprotein and/or its heme moiety due to the lack of substantial enzyme activity recovery following dialysis and chemical oxidation as well as the absence of the diagnostic Soret peak in spectral analyses.

We next sought to establish the identities of the reactive intermediate which could engender covalent modification of CYP3A. This was achieved by fortifying the reaction mixtures with saturating amounts of GSH, which serves to readily trap the labile reactive species generated *in situ* as stable conjugates and facilitate their eventual detection via the application of two complementary UPLC-MS/MS survey scans based on known GSH fragmentation patterns. These survey scans subsequently triggered the acquisition of two prospective GSH adducts (i.e., FUT-G1 and FUT-G2) that eluted very closely together which seemed to imply that they were structurally similar. However, as FUT contains an electrophilic acrylamide warhead which is known to be capable of directly conjugating to GSH via Michael addition (Schwöbel *et al.*, 2010), we were curious to discern if the GSH adducts profiled

DMD Fast Forward. Published on May 5, 2022 as DOI: 10.1124/dmd.122.000895
This article has not been copyedited and formatted. The final version may differ from this version.

earlier arose directly from FUT or indirectly through a reactive intermediate formed via metabolic activation of the parent compound. Strikingly, we demonstrated that when rhCYP3A4 was substituted with potassium phosphate buffer it resulted in the loss of the less abundant peak which corresponded to FUT-G2. This suggested that P450-mediated metabolic activation was a crucial step that culminated in the formation of FUT-G2. Our conjectures were proven to be correct in our high-resolution Orbitrap-MS analysis using a strict mass tolerance threshold of 5 ppm which enabled us to confidently establish that FUT-G1 was formed by the nonenzymatic conjugation of GSH to FUT via Michael addition whereas FUT-G2 resulted from an epoxide intermediate generated from P450-mediated metabolic activation of FUT at its acrylamide electrophilic warhead **(Fig. 8)**. Notably, the formation of FUT-G1 via direct GSH conjugation is similarly observed for other acrylamide-containing drugs and may play a significant role in its extrahepatic clearance although further pharmacokinetic studies are needed to evaluate its actual contribution (Shibata and Chiba, 2015). On the other hand, the formation of FUT-G2 is substantiated by a previous study which reported the *in vivo* P450-mediated epoxidation of acrylamide (Ghanayem *et al.*, 2005). Importantly, as we previously demonstrated that NADPH cofactor was necessary in order for FUT to evoke enzymatic inactivation, we believe that this epoxide metabolite was likely responsible for the covalent modification of the CYP3A. However, as our experiments did not yield direct evidence of covalent binding, future work involving MS-based proteomics methodologies are necessary to validate our postulations.

Targeted covalent inhibitors like FUT represent an emerging subcategory of tyrosine kinase inhibitors that typically possess an *α,β*-unsaturated carbonyl scaffold (i.e, acrylamide moiety) which allows it to covalently bind to a cysteine residue after the

DMD Fast Forward. Published on May 5, 2022 as DOI: 10.1124/dmd.122.000895
This article has not been copyedited and formatted. The final version may differ from this version.

molecule is tightly held in place within the active site by noncovalent interactions. This modality confers several attractive pharmacological advantages over conventional reversible ATP-competitive inhibitors such as an increased biochemical potency, a sustained duration of action and the potential to circumvent resistance arising through gatekeeper mutations (Carmi *et al.*, 2012; Kalgutkar and Dalvie, 2012). Although, such drugs present a hypothetical toxicological consideration arising from aberrant off-target covalent protein modification, this risk is mitigated by the low intrinsic electrophilicity of the acrylamide moiety which ensures that the covalent interaction can only ensue if the molecule is snuggly positioned within the binding pocket of its desired biological target. At present, a number of FDA-approved covalent inhibitors with acrylamide warheads (i.e., ibrutinib, osimertinib) are routinely utilized in the clinical setting and have demonstrated reasonable safety profiles. However, our study demonstrates that the acrylamide scaffold in targeted covalent inhibitors is amenable to be metabolically activated to a highly reactive epoxide intermediate. Due to its inherent ring strain, epoxides possess a greater electrophilic burden and can directly interact with DNA or cellular proteins to form adducts which may potentially induce mutagenicity and cytotoxicity (Ghanayem *et al.*, 2005). Although there are no current reports of idiosyncratic toxicities with FUT, our findings may serve as a premonitory indicator of reactive metabolite-induced toxicity. More importantly, as the relative abundances of these epoxide-derived GSH adducts (i.e., FUT-G2) tend to be eclipsed by those formed nonenzymatically (i.e, FUT-G1), it could masquerade as a single combined peak in UPLC-MS/MS survey scans and evade detection. Consequently, we advocate that closer scrutiny be adopted when profiling the reactive metabolites of compounds possessing an *α,β*-unsaturated carbonyl scaffold.

DMD Fast Forward. Published on May 5, 2022 as DOI: 10.1124/dmd.122.000895
This article has not been copyedited and formatted. The final version may differ from this version.

In conclusion, we established that FUT is an archetypal MBI of CYP3A. Furthermore, using FUT as an exemplary targeted covalent inhibitor, our study reveals the propensity for its acrylamide Michael acceptor to be metabolically activated to an epoxide which likely engendered covalent inactivation of CYP3A. The findings reported in this study are clinically-relevant due to the growing resurgence of therapeutic covalent inhibitors.

DMD Fast Forward. Published on May 5, 2022 as DOI: 10.1124/dmd.122.000895
This article has not been copyedited and formatted. The final version may differ from this version.

AUTHORSHIP CONTRIBUTIONS

Participated in research design:	Tang, Chan
Conducted experiments:	Tang, Fu, Koh, Wu
Contributed new reagents or analytical tools	Zhou
Performed data analysis:	Tang, Fu, Wu
Wrote or contributed to the writing of the manuscript:	Tang, Chan

DMD Fast Forward. Published on May 5, 2022 as DOI: 10.1124/dmd.122.000895
This article has not been copyedited and formatted. The final version may differ from this version.

BIBLIOGRAPHY

Baillie TA, and Davis MR (1993) Mass spectrometry in the analysis of glutathione conjugates. *Biol Mass Spectrom* **22**:319–325, Biol Mass Spectrom.

Bjornsson TD, Callaghan JT, Einolf HJ, Fischer V, Gan L, Grimm S, Kao J, King SP, Miwa G, Ni L, Kumar G, McLeod J, Obach RS, Roberts S, Roe A, Shah A, Snikeris F, Sullivan JT, Tweedie D, Vega JM, Walsh J, and Wrighton SA (2003) The conduct of in vitro and in vivo drug-drug interaction studies: A Pharmaceutical Research and Manufacturers of America (PhRMA) perspective. *Drug Metab Dispos* **31**:815–832.

Carmi C, Mor M, Petronini PG, and Alfieri RR (2012) Clinical perspectives for irreversible tyrosine kinase inhibitors in cancer. *Biochem Pharmacol* **84**:1388–1399, Elsevier.

Chakrabarti S, Finnes HD, and Mahipal A (2022) Fibroblast growth factor receptor (FGFR) inhibitors in cholangiocarcinoma: current status, insight on resistance mechanisms and toxicity management. *https://doi-org.libproxy1.nus.edu.sg/101080/1742525520222039118* 1–14, Taylor & Francis.

Dieckhaus CM, Fernández-Metzler CL, King R, Krolikowski PH, and Baillie TA (2005) Negative ion tandem mass spectrometry for the detection of glutathione conjugates. *Chem Res Toxicol* **18**:630–638, American Chemical Society .

Ghanayem BI, McDaniel LP, Churchwell MI, Twaddle NC, Snyder R, Fennell TR, and Doerge DR (2005) Role of CYP2E1 in the Epoxidation of Acrylamide to Glycidamide and Formation of DNA and Hemoglobin Adducts. *Toxicol Sci* **88**:311–318, Oxford Academic.

Goyal L, Meric-Bernstam F, Hollebecque A, Valle JW, Morizane C, Karasic TB, Abrams TA, Furuse J, He Y, Soni N, Benhadji KA, and Bridgewater JA (2020) FOENIX-CCA2: A phase II, open-label, multicenter study of futibatinib in patients (pts) with intrahepatic cholangiocarcinoma (iCCA) harboring FGFR2 gene fusions or other rearrangements. *https://doi.org/101200/JCO20203815_suppl108* **38**:108–108, American Society of Clinical Oncology.

Guengerich FP (2001) Common and Uncommon Cytochrome P450 Reactions Related to Metabolism and Chemical Toxicity. *Chem Res Toxicol* **14**:611–650, American Chemical Society .

Guengerich FP (2011) Mechanisms of drug toxicity and relevance to pharmaceutical development. *Drug Metab Pharmacokinet* **26**:3–14.

Helsten T, Elkin S, Arthur E, Tomson BN, Carter J, and Kurzrock R (2016) The FGFR landscape in cancer: Analysis of 4,853 tumors by next-generation sequencing. *Clin Cancer Res* **22**:259–267, American Association for Cancer Research Inc.

Ho HK, Chan JCY, Hardy KD, and Chan ECY (2015) Mechanism-based inactivation

of CYP450 enzymes: A case study of lapatinib. *Drug Metab Rev* **47**:21–28.

Kalgutkar AS, and Dalvie DK (2012) Drug discovery for a new generation of covalent drugs. *http://dx.doi.org.libproxy1.nus.edu.sg/101517/174604412012688744* **7**:561–581, Taylor & Francis.

Kalgutkar AS, R. Scott Obach, and Tristan S. Maurer (2007) Mechanism-Based Inactivation of Cytochrome P450 Enzymes: Chemical Mechanisms, Structure-Activity Relationships and Relationship to Clinical Drug-Drug Interactions and Idiosyncratic Adverse Drug Reactions. *Curr Drug Metab* **8**:407–447, Curr Drug Metab.

Kitz R, and Wilson IB (1962) Esters of methanesulfonic acid as irreversible inhibitors of acetylcholinesterase. *J Biol Chem* **237**:3245–3249.

Lim HK, Duczak N, Brougham L, Elliot M, Patel K, and Chan K (2005) Automated screening with confirmation of mechanism-based inactivation of CYP3A4, CYP2C9, CYP2C19, CYP2D6, and CYP1A2 in pooled human liver microsomes. *Drug Metab Dispos* **33**:1211–1219.

Masubuchi Y, and Horie T (2007) Toxicological significance of mechanism-based inactivation of cytochrome P450 enzymes by drugs, Taylor & Francis.

Nassar AF, Hollenberg PF, and Scatina J (2008) *Drug Metabolism Handbook: Concepts and Applications*.

Orr STM, Ripp SL, Ballard TE, Henderson JL, Scott DO, Obach RS, Sun H, and Kalgutkar AS (2012) Mechanism-based inactivation (MBI) of cytochrome P450 enzymes: Structure-activity relationships and discovery strategies to mitigate drug-drug interaction risks. *J Med Chem* **55**:4896–4933.

Polasek TM, and Miners JO (2008) Time-dependent inhibition of human drug metabolizing cytochromes P450 by tricyclic antidepressants. *Br J Clin Pharmacol* **65**:87–97.

Porta R, Borea R, Coelho A, Khan S, Araújo A, Reclusa P, Franchina T, Van Der Steen N, Van Dam P, Ferri J, Sirera R, Naing A, Hong D, and Rolfo C (2017) FGFR a promising druggable target in cancer: Molecular biology and new drugs. *Crit Rev Oncol Hematol* **113**:256–267, Elsevier.

Schwöbel JAH, Wondrousch D, Koleva YK, Madden JC, Cronin MTD, and Schüürmann G (2010) Prediction of michael-type acceptor reactivity toward glutathione. *Chem Res Toxicol* **23**:1576–1585, American Chemical Society.

Shibata Y, and Chiba M (2015) The role of extrahepatic metabolism in the pharmacokinetics of the targeted covalent inhibitors afatinib, ibrutinib, and neratinib. *Drug Metab Dispos* **43**:375–384.

Silverman RB (1995) Mechanism-based enzyme inactivators. *Methods Enzymol* **249**:240–283.

Sootome H, Fujita H, Ito Kenjiro, Ochiiwa H, Fujioka Y, Ito Kimihiro, Miura A, Sagara T, Ito S, Ohsawa H, Otsuki S, Funabashi K, Yashiro M, Matsuo K, Yonekura K, and Hirai H (2020) Futibatinib Is a Novel Irreversible FGFR 1–4 Inhibitor That

Shows Selective Antitumor Activity against FGFR-Deregulated Tumors. *Cancer Res* **80**:4986–4997.

Tang LWT, and Chan ECY (2022) Quantification of the Irreversible Fibroblast Growth Factor Receptor Inhibitor Futibatinib by UPLC-MS/MS: Application to the Metabolic Stability Assay in Human Liver Microsomes for the Estimation of its In Vitro Hepatic Intrinsic Clearance. *J Pharm Biomed Anal* **214**:114731, Elsevier B.V.

Tang LWT, Teng JW, Koh SK, Zhou L, Go ML, and Chan ECY (2021a) Mechanism-Based Inactivation of Cytochrome P450 3A4 and 3A5 by the Fibroblast Growth Factor Receptor Inhibitor Erdafitinib. *Chem Res Toxicol* **34**:1800–1813.

Tang LWT, Teng JW, Verma RK, Koh SK, Zhou L, Go ML, Fan H, and Chan ECY (2021b) Infigratinib Is a Reversible Inhibitor and Mechanism-Based Inactivator of Cytochrome P450 3A4. *Drug Metab Dispos* **49**:856–868, American Society for Pharmacology and Experimental Therapeutics.

Tang LWT, Verma RK, Fan H, and Chan ECY (2021c) Mechanism-Based Inactivation of Cytochrome P450 3A4 by Benzbromarone. *Mol Pharmacol* **99**:266–276, American Society for Pharmacology and Experimental Therapeutics.

Tang LWT, Wei W, Verma RK, Koh SK, Zhou L, Fan H, and Chan ECY (2022) Direct and Sequential Bioactivation of Pemigatinib to Reactive Iminium Ion Intermediates Culminate in Mechanism-Based Inactivation of Cytochrome P450 3A. *Drug Metab Dispos* DMD-AR-2021-000804, American Society for Pharmacology and Experimental Therapeutics.

Touat M, Ileana E, Postel-Vinay S, André F, and Soria JC (2015) Targeting FGFR signaling in cancer. *Clin Cancer Res* **21**:2684–2694, American Association for Cancer Research.

Watanabe A, Nakamura K, Okudaira N, Okazaki O, and Sudo KI (2007) Risk assessment for drug-drug interaction caused by metabolism-based inhibition of CYP3A using automated in vitro assay systems and its application in the early drug discovery process. *Drug Metab Dispos* **35**:1232–1238.

Yamamiya I, Laabs J, Hunt A, Takenaka T, Sonnichsen D, Mina M, He Y, and Benhadji K (2021) Abstract CT125: Evaluation of potential drug-drug interactions (DDIs) between futibatinib and CYP3A inhibitors/inducers, CYP3A substrates, or proton pump inhibitors (PPIs). *Cancer Res* **81**:CT125–CT125, American Association for Cancer Research.

Zanger UM, Turpeinen M, Klein K, and Schwab M (2008) Functional pharmacogenetics/genomics of human cytochromes P450 involved in drug biotransformation.

Zimmerlin A, Trunzer M, and Faller B (2011) CYP3A Time-Dependent Inhibition Risk Assessment Validated with 400 Reference Drugs. *Drug Metab Dispos* **39**:1039–1046, American Society for Pharmacology and Experimental Therapeutics.

FOOTNOTES

L.W.T.T is supported by the National University of Singapore (NUS) President's Graduate Fellowship (PGF). This work was supported by the Singapore Ministry of Education Tier 1 Academic Research Funding [Grant: A-0008501-00-00] to E.C.Y.C.

The authors declare that they have no conflicts of interest with the contents of this article.

DMD Fast Forward. Published on May 5, 2022 as DOI: 10.1124/dmd.122.000895
This article has not been copyedited and formatted. The final version may differ from this version.

FIGURE LEGENDS

Fig. 1. Chemical structure of futibatinib (FUT).

Fig. 2. Substrate depletion of FUT by CYP3A. Percentage of FUT remaining against time in the presence of (A) CYP3A4 and (B) CYP3A5 plotted on a linear scale and the corresponding substrate depletion graphs of FUT in (C) CYP3A4 and (D) CYP3A5 as plotted on a semi-log scale. Each point in (A to D) represents the mean and S.D. of triplicate experiments.

Fig. 3. (A) Time- and concentration-dependent inactivation of CYP3A4-mediated rivaroxaban hydroxylation by FUT. (B) Nonlinear least square regression of k_{obs} versus various concentrations of FUT yielded K_I and k_{inact} values of 12.5 ± 2.4 μM and 0.25 ± 0.02 min^{-1}. (C) Inactivation of CYP3A4 by FUT also exhibited cofactor-dependency. Each point in (A to C) represents the mean and S.D. of triplicate experiments.

Fig. 4. (A) Partition ratio for the inactivation of CYP3A4 by FUT was estimated to be 52, implying that enzyme inactivation was efficient. Inactivation of CYP3A4 was diminished by coincubation with (B) an alterative CYP3A substrate (testosterone) and considerably abrogated by (C) a direct inhibitor of CYP3A (ketoconazole). (D) On the contrary, the inclusion of either an exogenous nucleophile (GSH) or a scavenger of ROS (catalase) did not confer substrate protection. Each point in (A to D) represents the mean and S.D. of triplicate experiments.

Fig. 5. Metabolic activity of CYP3A4 was (A) not restored after extensive dialysis at 4°C for 4 h and (B) only modestly restored by 1.3 ± 0.3% following treatment with 2 mM potassium ferricyanide (KFC). (C) Absorbance difference measured over 1 h failed to detect a spectrally resolvable peak in the Soret region (448 – 458 nm) for

DMD Fast Forward. Published on May 5, 2022 as DOI: 10.1124/dmd.122.000895
This article has not been copyedited and formatted. The final version may differ from this version.

CYP3A4 incubated with FUT. (D) Likewise, a comparison of the absorbance at the reference of 454 nm against the isosbestic point at 490 nm failed to demonstrate an increase in the extent of MIC formation over time. Results from (A and B) depict the mean and S.D. of three independent experiments conducted in triplicates.

Fig. 6. Total ion chromatogram for PIS of *m/z* 272 in negative ESI mode of (A) vehicle, (B) FUT (rhCYP3A4) and (C) FUT buffer (enzyme-free) incubation mixtures fortified with 50 mM GSH. Total ion chromatogram for constant NL scan of 129 Da in positive ESI mode of the same aforementioned (D) vehicle, (E) FUT (rhCYP3A4) and (F) FUT buffer (enzyme-free) incubation mixtures. Notably, while a peak corresponding to the FUT-derived GSH adduct FUT-G1 (retention time: 6.32 min) was detected in both survey scans for incubation mixture comprising FUT, an additional but less abundant GSH adduct FUT-G2 (retention time: 6.24 min) was present only in FUT incubation mixtures that contained rhCYP3A4 and absent in FUT buffer incubation mixtures.

Fig. 7. (A) Representative product ion chromatogram of (A) FUT-G1 and (B) FUT-G2. Proposed accurate mass fragmentation pattern of (C) FUT-G1 and (D) FUT-G2. The exact mass MS/MS spectra depict the experimental *m/z* values whereas the chemical structures (inset) illustrate the theoretical accurate *m/z* values of the parent and product ions of the two GSH adducts formed *in situ* in the GSH trapping assay as outlined in Table 2 and 3 using a strict mass tolerance cutoff of ≤5 ppm.

Fig. 8. Proposed chemical pathway for the formation of the GSH conjugates FUT-G1 and FUT-G2. FUT-G1 is formed by the nonenzymatic conjugation of GSH to FUT via Michael addition whereas FUT-G2 is formed via the nucleophilic attack of GSH to an

DMD Fast Forward. Published on May 5, 2022 as DOI: 10.1124/dmd.122.000895
This article has not been copyedited and formatted. The final version may differ from this version.

epoxide intermediate generated from P450-mediated metabolic activation of FUT at its acrylamide electrophilic warhead.

Table 1. CYP3A4 and CYP3A5 inactivation kinetic parameters for FUT derived using morpholinone hydroxylation of rivaroxaban as an *in vitro* marker reaction of residual CYP3A activity. Data are presented as means ± S.D.

P450 Isoform	**K_I (μM)**	**k_{inact} (min^{-1})**	**k_{inact}/K_I ($min^{-1}mM^{-1}$)**	**$t_{1/2}$ (min)**	**Partition Ratio**
CYP3A4	12.5 ± 2.4	0.25 ± 0.02	20.0	2.8	52
CYP3A5	51.4 ± 21.4	0.06 ± 0.02	1.2	11.6	58

DMD Fast Forward. Published on May 5, 2022 as DOI: 10.1124/dmd.122.000895
This article has not been copyedited and formatted. The final version may differ from this version.

Table 2. Accurate mass measurement of the parent and product ions of FUT-G1 using a mass tolerance cutoff of ≤5 ppm.

Proposed Elemental Composition	**Theoretical *m/z***	**Experimental *m/z***	**Mass Accuracy**	
			∆Da	**∆ppm**
$C_{32}H_{40}O_9N_9S$	726.2664	726.2629	-0.0035	-4.8
$C_{32}H_{38}O_8N_9S$	708.2559	708.2528	-0.0031	-4.4
$C_{27}H_{33}O_6N_8S$	597.2238	597.2212	-0.0026	-4.4
$C_{19}H_{21}O_2N_6$	365.1721	365.1704	-0.0017	-4.7

DMD Fast Forward. Published on May 5, 2022 as DOI: 10.1124/dmd.122.000895
This article has not been copyedited and formatted. The final version may differ from this version.

Table 3. Accurate mass measurement of the parent and product ions of FUT-G2 using a mass tolerance cutoff of ≤5 ppm.

Proposed Elemental Composition	**Theoretical *m/z***	**Experimental *m/z***	**Mass Accuracy**	
			∆Da	**∆ppm**
$C_{32}H_{40}O_{10}N_9S$	742.2613	742.2627	0.0014	1.9
$C_{32}H_{38}O_9N_9S$	724.2508	724.2473	-0.0035	-4.8
$C_{32}H_{36}O_8N_9S$	706.2402	706.2370	-0.0034	-4.8
$C_{27}H_{33}O_7N_8S$	613.2187	613.2159	-0.0028	-4.6
$C_{27}H_{31}O_6N_8S$	595.2082	595.2055	-0.0027	-4.5
$C_{15}H_{14}O_2N_5$	296.1142	296.1127	-0.0015	-5.0

DMD Fast Forward. Published on May 5, 2022 as DOI: 10.1124/dmd.122.000895
This article has not been copyedited and formatted. The final version may differ from this version.

Table 4. Comparison of the CYP3A4 enzyme inactivation kinetic parameters between FUT and the other FDA-approved FGFR inhibitors using morpholinone hydroxylation of rivaroxaban as an *in vitro* marker reaction of residual CYP3A activity

Compound	K_I (μM)	k_{inact} (min^{-1})	k_{inact}/K_I (min^{-1} mM^{-1})	Partition Ratio	Reference
FUT	12.5	0.25	20.0	52	
Erdafitinib	4.0	0.12	30.0	32	(Tang *et al.*, 2021a)
Infigratinib	4.2	0.07	16.7	41	(Tang *et al.*, 2021b)
Pemigatinib	8.7	0.11	12.6	44	(Tang *et al.*, 2022)

DMD Fast Forward. Published on May 5, 2022 as DOI: 10.1124/dmd.122.000895
This article has not been copyedited and formatted. The final version may differ from this version.

Figure 1

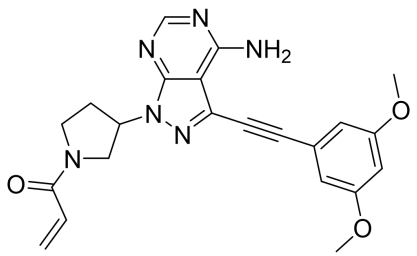

Futibatinib (FUT)

DMD Fast Forward. Published on May 5, 2022 as DOI: 10.1124/dmd.122.000895
This article has not been copyedited and formatted. The final version may differ from this version.

Figure 2

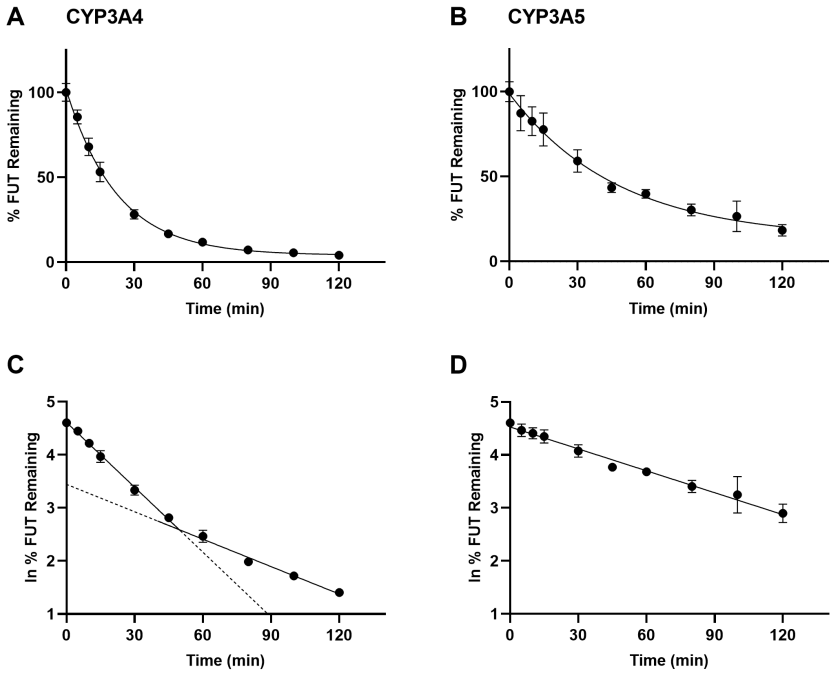

DMD Fast Forward. Published on May 5, 2022 as DOI: 10.1124/dmd.122.000895
This article has not been copyedited and formatted. The final version may differ from this version.

Figure 3

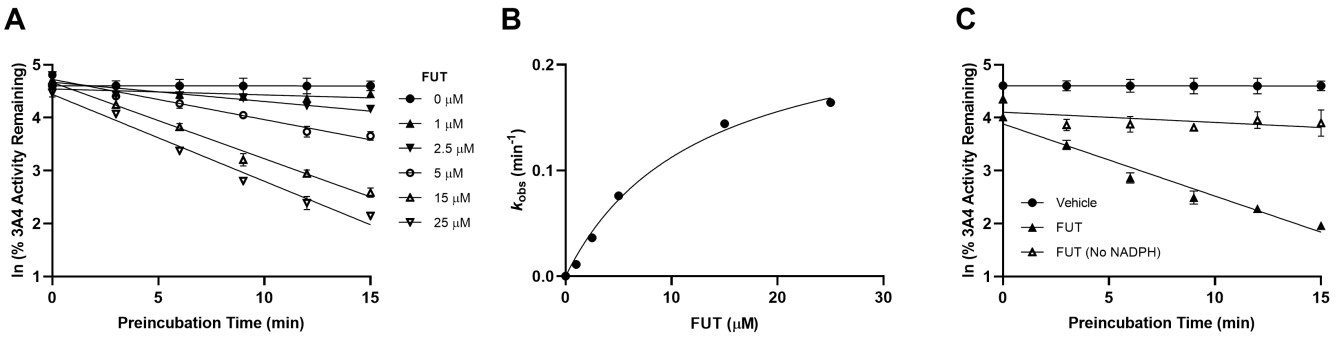

DMD Fast Forward. Published on May 5, 2022 as DOI: 10.1124/dmd.122.000895
This article has not been copyedited and formatted. The final version may differ from this version.

Figure 4

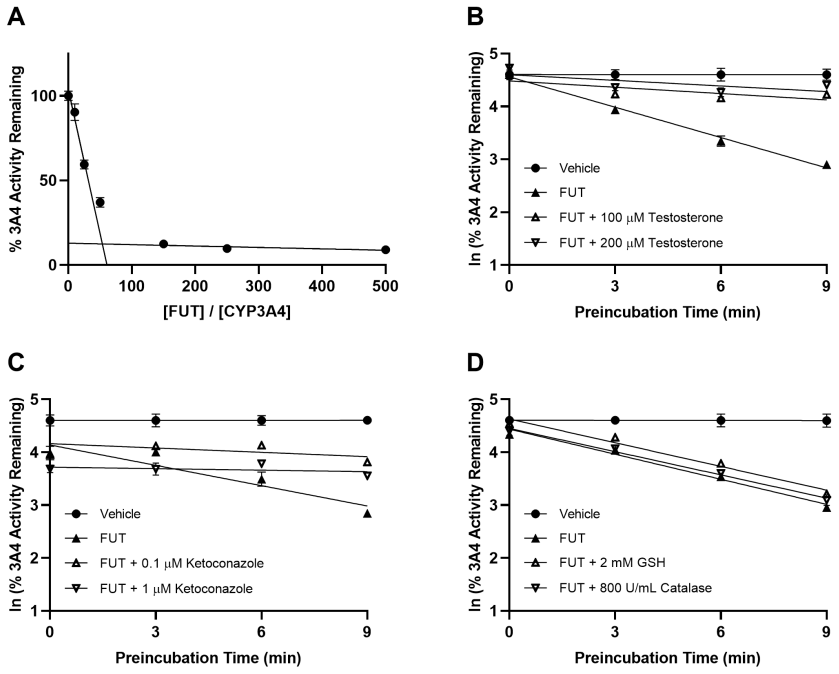

DMD Fast Forward. Published on May 5, 2022 as DOI: 10.1124/dmd.122.000895
This article has not been copyedited and formatted. The final version may differ from this version.

Figure 5

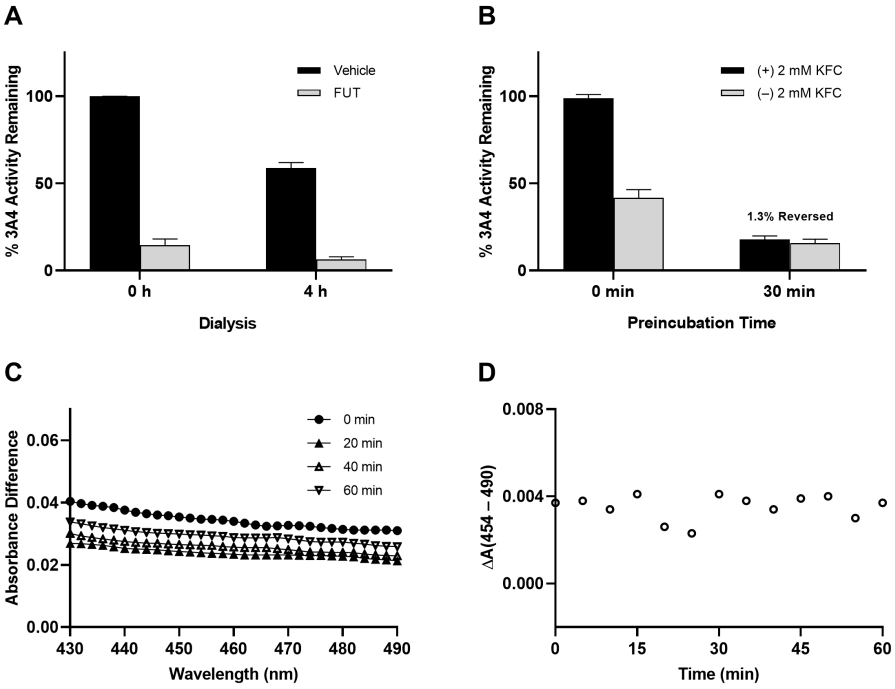

DMD Fast Forward. Published on May 5, 2022 as DOI: 10.1124/dmd.122.000895
This article has not been copyedited and formatted. The final version may differ from this version.

Figure 6

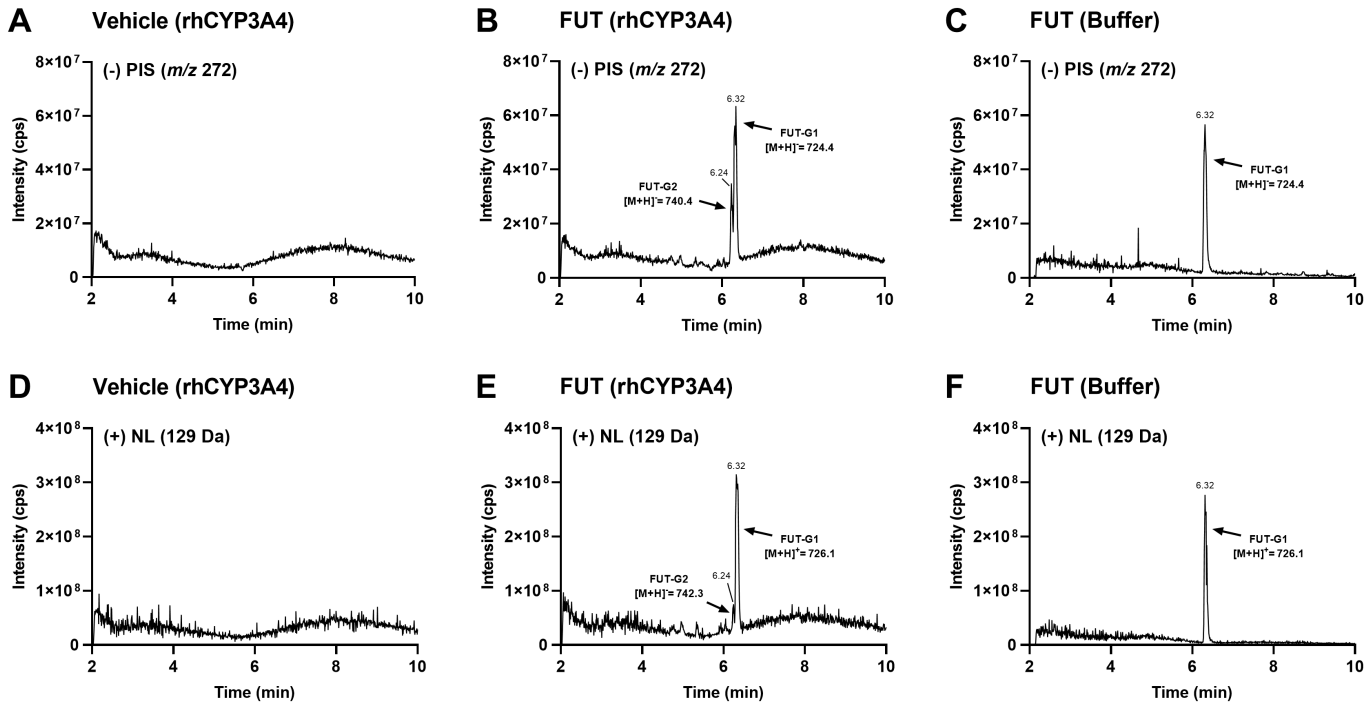

DMD Fast Forward. Published on May 5, 2022 as DOI: 10.1124/dmd.122.000895
This article has not been copyedited and formatted. The final version may differ from this version.

Figure 7

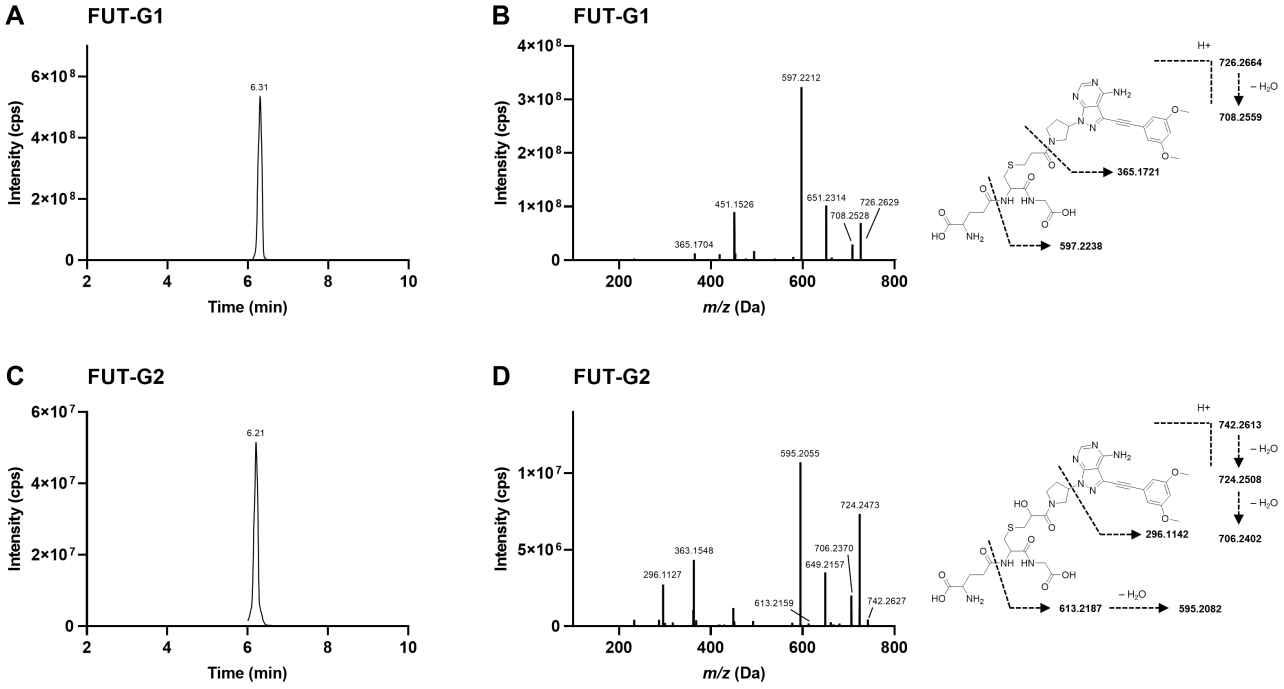

DMD Fast Forward. Published on May 5, 2022 as DOI: 10.1124/dmd.122.000895
This article has not been copyedited and formatted. The final version may differ from this version.

Figure 8